Experimental Characteristics of Crossed-Field Space-Charge Flows*

N. A. MASNARI AND J. E. ROWE

Electron Physics Laboratory, Department of Electrical Engineering,
The University of Michigan, Ann Arbor, Michigan

(Received 12 May 1965; in final form 29 November 1965)

An experimental method is described for determining the characteristics of space-charge flow in crossed electric and magnetic fields. A beam-intercepting system, which consists of a movable grid of wires biased at appropriate potentials, is inserted across the space-charge flow. The currents intercepted by the wires provide a description of the beam profile at each cross section of the electron beam. Evaluation of the data indicated that in no case did the beam assume a scalloped configuration. In general, it was found that the entire beam undulates in a serpentine manner and has variable thickness throughout the region of interest. The experimental undulation is observed to be in good agreement with the theoretical cycloidal wavelength for electron motion in a crossed-field environment. Calculations of space-charge density indicate that the average value is generally between 0.5 and 1.5 times the Brillouin space-charge density in each case.

INTRODUCTION

THE flow of electrons in orthogonal static electric and magnetic fields has been utilized in many experiments and devices in both cylindrical and planar configurations. An interesting class of crossed-field electron guns utilizing planar geometry and giving rectangular electron beams is the subject of an experimental investigation herein outlined. In particular it is desired to determine the beam profiles and current-density variations as a function of voltage and magnetic field.

In cylindrical electron beams confined by static axial magnetic fields there is very little voltage variation across the beam as it moves through a drift region. Thus it is possible to insert a unipotential aperture plate transverse to the space-charge flow without distorting the beam to any significant extent. The amount of current passing through the aperture is proportional to the current density in the beam at that point. By moving the aperture across the beam it is possible to determine the beam profile at a given cross section. Similar measurements at different cross sections along the beam provide a fairly complete record of the beam variations in density and cross-sectional area in the region of interest. The velocity distribution of the electrons in the beam can be obtained by the use of a Faraday cage system.[1]

Unfortunately, the voltage varies significantly across the beam in a crossed-field system since a strong transverse electric field is required to balance the magnetic force on the electrons. Thus, it is not possible to insert a unipotential aperture plate across the beam without greatly disturbing the characteristics of the space-charge flow. Consequently it is necessary to revert to other measurement systems to obtain the characteristics of space-charge flows in crossed electric and magnetic fields.

The crossed-field electron flow which has been the subject of most investigations is that which exists in the cylindrical magnetron. Independent experimental investigations were carried out by Reverdin[2] and Peterson[3] in which the cathode–anode space was probed by means of an axially directed electron beam probe. The probing beam was passed through the space-charge region and the resulting pattern displayed on a fluorescent screen. The results indicated the existence of space charge (secular space charge) outside of the theoretical Brillouin limit. Mathias,[4] using a cesium fluoride molecular beam, and Nedderman,[5] using helium and hydrogen probes, obtained results similar to the Reverdin and Peterson data.

An electron-beam analyzer has been used to study the characteristics of space-charge flows in planar systems. A grid of wires is placed transverse to the flow direction of the electron beam in the planar interaction region (anode–sole region) and is movable along the z direction (general direction of motion of the electrons). Each wire is biased to a potential which corresponds approximately to the voltage at that location in the interaction region so that the complete grid exerts only a small disturbance on the electron beam. The currents intercepted by the grid wires thus indicate the beam profile at a given cross section. Movement of the grid system along the z direction yields a description of the beam profile variation in the anode–sole region.

The experimental results obtained from the beam analyzer investigations are presented below and analyzed. In particular the measurements of beam profiles in the interaction region are described in detail. Comparisons are made with theoretical work wherever possible.

DESCRIPTION OF EXPERIMENTAL BEAM ANALYZER

The investigation of the space-charge flow characteristics has been carried out by making use of an electron-

[1] C. C. Cutler, and J. A. Saloom, Proc. IRE 43, 299 (1955).

[2] D. L. Reverdin, J. Appl. Phys. 22, 257 (1951).
[3] W. W. Peterson, Tech. Report No. 18, Electron Tube Laboratory, The University of Michigan, Ann Arbor, May, 1954.
[4] L. Mathias, J. Electron. 1, 8 (1955).
[5] H. C. Nedderman, J. Appl. Phys. 26, 1420 (1955).

beam analyzer which consists of four basic units: (1) a vacuum system capable of achieving pressures of at least 10^{-8} Torr, (2) a base chamber and bell jar within which the experimental configuration is located, (3) a movable electron-beam interception system, and (4) a mechanical system for moving the measurement apparatus.

The experimental structure, which consists of an electron gun and planar anode–sole region, is attached to the stationary base plate. The beam interception system is mounted on a movable center pedestal which is brought into the base chamber through a flexible bellows. High-current feedthroughs mounted on the side walls of the base chamber are used to provide electrical connections to the device under investigation. The configuration to be studied consists of an extended Kino short gun,[6] planar anode–sole region (0.130-in. spacing between anode and sole) and a V-shaped copper collector block.

The grid assembly consists of 10 parallel 0.003-in.-diam tungsten wires stretched across a frame which is mounted to the movable center pedestal. The spacing between grid wires is approximately 0.010 in. Each wire is connected to one of the terminals on the feedthroughs so that voltages can be applied to the various wires by connecting to the appropriate terminal on the external base plate connection panel.

For the investigations described herein the motion of the grid wires is restricted to the z direction (i.e., parallel to the anode and sole electrodes).

EXPERIMENTAL RESULTS

Beam-Profile Investigations

The experimental beam-analyzer investigations are concerned with the evaluation of the behavior of the electron beam as it moves through a planar anode–sole region. In particular the investigations are intended to evaluate the manner in which the beam thickness, beam location, and current density vary in the z direction. The investigations have been primarily concerned with the electron beams formed by an extended Kino short gun as illustrated in Fig. 1. The anode and collector are
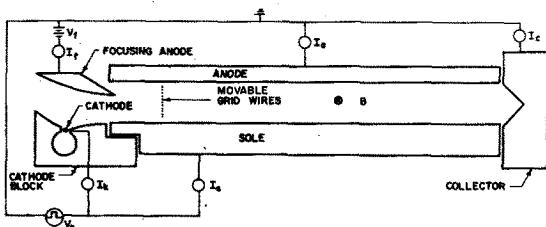
FIG. 1. Schematic diagram of the extended Kino gun crossed-field device.

[6] G. S. Kino, IRE Trans. *PGED* ED-7, 179 (1960).
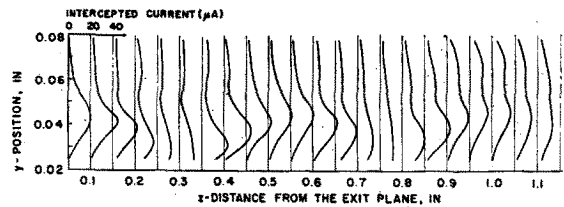[7] R. J. Martin, N. A. Masnari, and J. E. Rowe, IRE Trans. *PGEC* 9, 490 (1960).

FIG. 2. Currents intercepted by the grid wires at various cross sections in the interaction region. ($\varphi_f = 925$ V, $\varphi_a = 1425$ V, $B = 352$ G.)

maintained at ground potential while the cathode and sole are pulsed between ground and a negative voltage V_c. Pulsed operation is used to eliminate thermal problems created by the excessive heat dissipation. The pulser generates 100-μsec pulses at the rate of 100 pps. The focusing anode is biased at a voltage V_f by means of a dc supply. The work which follows is discussed using the cathode potential as the reference, i.e., $\varphi_k = 0$. Thus the anode, focusing anode, and sole voltages are expressed as $\varphi_a = -V_c$, $\varphi_f = V_f - V_c$, and $\varphi_s = 0$, respectively.

The determination of the gross characteristics of the electron beam in the planar anode–sole region is accomplished by intercepting the beam with a grid of wires. The grid wire assembly is located so that the ten wires lie in a plane which is transverse to the general direction of electron flow as indicated in Fig. 1. The voltage is applied to each wire by connection to a series network of 11 resistors whose two terminals are connected to the sole and anode potential, respectively. In the absence of a beam, the voltage on each wire is the space-charge-free voltage corresponding to that location in the device. However, in the presence of a beam, some of the beam current arrives at the wires and flows through the resistance network. This results in the voltage on each wire being reduced in much the same manner as the actual voltage at each point is changed due to the presence of the beam.

The magnitude of current intercepted by a given wire depends on the current density at that point as well as on the potential difference between the wire and the corresponding location in the beam. If it is assumed that this potential difference is relatively small, (i.e., the resistors in the network are so chosen that the intercepted currents modify the potentials of the wires in the desired manner) then the currents intercepted by the wires provide a description of the beam profile. The variation of the beam profile throughout the interaction region can be observed by moving the grid system and monitoring the current interceptions at the various cross sections.

Figure 2 illustrates the profile variations obtained for $\varphi_f = 925$ V, $\varphi_a = 1425$ V and $B = 352$ G. It is obvious from Fig. 2 that the beam is undergoing periodic variation as it proceeds through the anode–sole region. The periodic behavior is more apparent in Fig. 3 where the y location of the maximum current interception has been

plotted for each z position of the grid wires. The result indicates a distance of approximately 0.48 in. between successive maxima and 0.46 in. between minima. The theoretical cycloidal wavelength of an electron in a planar anode–sole region can be written as

$$L_{th} = 2\pi \varphi_{a-s}/\eta d B^2, \qquad (1)$$

where φ_{a-s} is the potential difference between the anode and the sole, and d is the anode–sole spacing. Although Eq. (1) is exactly correct only for the space-charge-free case, it is a very good approximation for a rippling beam since the average electric field in such a beam is nearly the same as the space-charge-free value. Substituting the appropriate values of Fig. 2 into the above results in $L_{th} = 0.496$ in., which is in reasonable agreement with the experimental values.

The undulation of the beam under high magnetic field conditions is illustrated in Fig. 4 for $\varphi_f = 1360$ V, $\varphi_a = 2210$ V, and $B = 590$ G. Obviously, the magnetic field has caused the beam to pass rather close to the sole
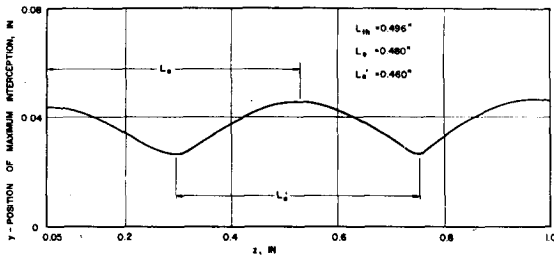

FIG. 3. Location of maximum current interception at various z positions. ($\varphi_f = 925$ V, $\varphi_a = 1425$ V, $B = 352$ G.)

electrode such that at its minimum location very little current strikes the grid wires. Once again there is good agreement between the theoretical and experimental values of the period ($L_{th} = 0.276$ in., $L_0 = 0.290$ in.). The maximum current intercepted at any cross section appears to increase with z, which implies an increase in either the space-charge density or the beam velocity. However, the behavior is not sufficiently consistent to allow definite conclusions to be drawn. For example, in Fig. 2 the opposite behavior was observed such that the maximum current interception decreased with increasing z, while simultaneously the beam became wider and less clearly defined.

Figure 5 illustrates another situation in which the beam undergoes appreciable undulation for the conditions $\varphi_f = 1105$ V, $\varphi_a = 1765$ V, and $B = 465$ G. The reason for the undulation is seen from investigating the electric field and electron velocities at the gun-exit plane and comparing with those in the interaction region. Assuming that the beam does not modify the potential distribution significantly from the space-charge-free value, the electric fields are found to be

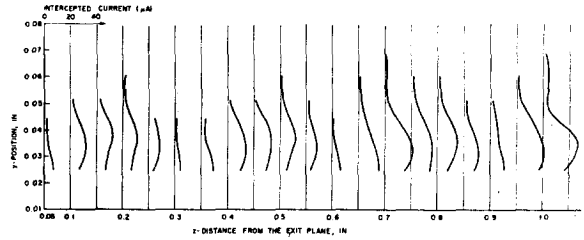$$(E) \text{ gun exit} = 5.15 \times 10^5 \text{ V/m}$$

FIG. 4. Currents intercepted by the grid wires at various cross sections in the interaction region. ($\varphi_f = 1360$ V, $\varphi_a = 2210$ V, $B = 590$ G.)

and

$$(E) \text{ anode–sole} = 5.42 \times 10^5 \text{ V/m}.$$

The velocity of the electrons at the gun exit is

$$v = 1.02 \times 10^7 \text{ m/sec},$$

whereas E/B in the interaction region is

$$E_{a-s}/B = 1.16 \times 10^7 \text{ m/sec}.$$

Thus there are two factors which contribute to the perturbation of the beam as it enters the interaction region: first, the velocity of the incoming electrons (1.02×10^7 m/sec) is less than the desired value (1.16×10^7 m/sec); and second, the anode–sole region electric field exceeds the exit-plane value. Both of these conditions result in the entering electrons experiencing an upward-directed force causing them to move toward the anode, as indicated in Fig. 5.

The preceding experimental results have been interpreted neglecting the effect of the grid wires on the beam. This effect can be evaluated qualitatively by referring to Fig. 6 which indicates the results when grid wire 4 was disconnected from the resistance network with $\varphi_f = 900$ V, $\varphi_a = 1490$ V, and $B = 352$ G (these operating conditions are comparable to those of Fig. 2). Although wire 4 draws no current, the profiles are plotted as if $I_4 \neq 0$ in order to make the profile variation easier to analyze. It is interesting to observe that the same type of behavior occurs here as when wire 4 is connected to the circuit in the usual manner (see Fig. 2).

Figure 7 presents a detailed description of the currents intercepted by wire 3, both with wire 4 connected
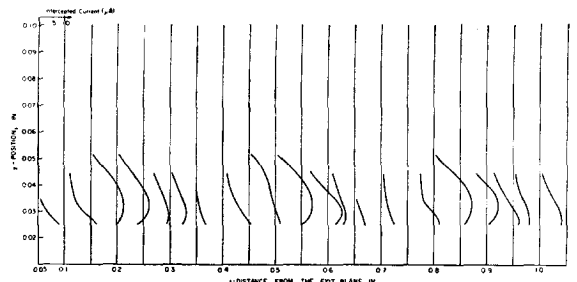

FIG. 5. Currents intercepted by the grid wires at various cross sections. ($\varphi_f = 1105$ V, $\varphi_a = 1765$ V, $B = 465$ G.)
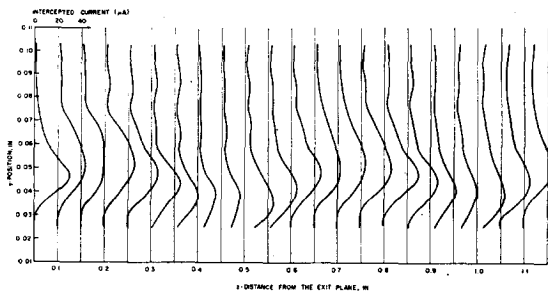
FIG. 6. Currents intercepted by the grid wires at various cross sections of the interaction region with wire no. 4 disconnected. ($\varphi_f = 990$ V, $\varphi_a = 1490$ V, $B = 352$ G.)

and disconnected. The experimental points were obtained by moving the grid assembly along the z axis in increments of 0.01 in. The I_3 variation is the same in each case except that the magnitude of the intercepted current is greater with wire 4 disconnected. This implies that the presence of the grid wires does not distort the beam as far as the general configuration and periodic variation are concerned. The difference in the value of intercepted current comes about as a result of the potential on wire 3 being affected by the disconnection of wire 4. When wire 4 is disconnected, its intercepted current no longer flows through the resistance network, thus resulting in an initial increase in the voltage on wire 3. However, as V_3 increases, it draws more electrons until a new equilibrium condition is reached with a correspondingly higher current in wire 3. Thus the magnitude of current interception depends not only on the current density but also on the difference in potential between the wire and the corresponding beam location.

The experimental value of the cycloidal wavelength is obtained by measuring the distance between alternate peaks in Fig. 7 rather than adjacent peaks. This is necessary because of the wavelike nature of the maximum current-interception locus. In other words, since the position of the maximum current varies periodically, it is obvious that the cyclotron wavelength corresponds to the distance between alternate points of intersection of the wave and any constant y line.

It is difficult to obtain an exact description of the beam from the experimental data. However, if the beam
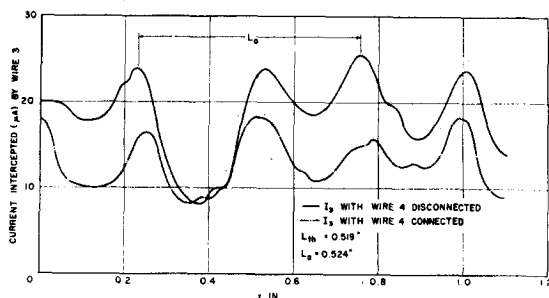

FIG. 7. Comparison of the currents intercepted by wire 3 when wire 4 is connected and disconnected. ($\varphi_f = 990$ V, $\varphi_c = 1490$ V, $B = 352$ G.)

is defined to lie between those points where the intercepted current is 10% of that at the maximum profile point, then it is possible to plot a beam configuration in the anode–sole region. Figure 8 represents a typical beam profile obtained in this manner ($\varphi_f = 1105$ V, $\varphi_a = 1765$ V, $B = 295$ G). Figure 8 also includes information on the location and thickness of the Brillouin beam which is compatible with the experimental voltages, current, and magnetic field. The experimental beam enters the anode–sole region far below the corresponding Brillouin beam location. The effect of such an entrance is to produce a greater electric field on the top edge of the beam, thus resulting in the sharp upward curvature of the electron trajectories. This is followed by the usual cycloidal variation of the beam. There is also a pronounced beam thickness variation, with the largest width occurring when the beam is at its maximum height above the sole.

The beam configuration illustrated in Fig. 8 is typical of the results obtained under various operating conditions. The beam generally is thicker than the corre-
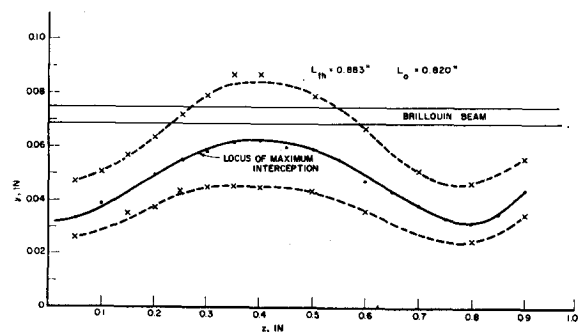

FIG. 8. Experimental beam configuration in the interaction region. ($\varphi_f = 1105$ V, $\varphi_a = 1765$ V, $B = 295$ G.)

sponding Brillouin beam and its location varies periodically while the thickness either varies in a periodic manner or remains approximately constant. Under no condition was a scalloped beam obtained, i.e., a beam whose average position is fixed but whose thickness varies periodically. However, since these experiments were performed with a planar anode in the interaction region one must be careful in generalizing the results to other situations. For example, the insertion of an rf structure, such as an interdigital line, into the interaction region might result in the establishment of a scalloped electron beam.

Another factor which influences the shape of the apparent beam profile is the emission of secondary electrons from any surface which is bombarded by primary electrons. Figure 9 compares the linear current-density distribution in a Brillouin beam with a profile which is typical of the experimental observations. The secondary electrons released from one wire are capable of moving to higher potential wires. This situation is possible because most of the secondaries are emitted in the negative

FIG. 9. Comparison of the theoretical Brillouin current density distribution with a typical experimental profile.
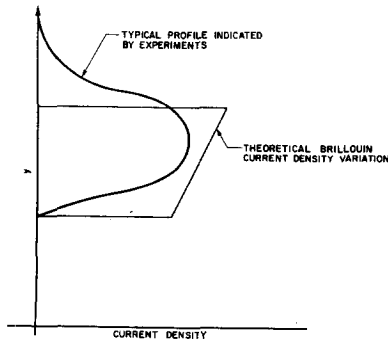
z direction with several electron volts of energy. The electric and magnetic fields act to reverse the z-directed motion of the electrons while forcing them to move toward the anode. Thus some of the secondary electrons can reach wires located above that from which they originated. Higher secondary-electron energy will allow electrons to reach even higher y positions in the plane of the grid wires. Thus if a Brillouin beam strikes the grid, the net current reading of the lowest potential wire will be reduced due to its loss of secondary electrons. Similarly the uppermost wire which is struck by the beam will eject secondaries which move through the beam boundary and arrive at wires located above the space-charge flow. The secondary currents reaching these wires would imply a beam width greater than the actual value. They would also impart a rounded shape to the apparent beam profile as determined from the current interception data. Both of these characteristics are typical of the experimental beam configurations described above. Since it is necessary to intercept the beam in order to determine its characteristics, the secondary emission problem is difficult to avoid. Thus the measurement technique introduces some uncertainty into the beam profile calculations.

It is interesting to compare the beam analyzer results with those obtained from other investigations. Figure 10 illustrates the over-all space-charge flow in a device utilizing an extended Kino short gun. The beam outline in the gun region was obtained from an analog computer

FIG. 10. Comparison of experimental beam analyzer results with the electron beam configuration obtained from a Poisson cell analysis.

analysis using a Poisson cell[7] with the operating conditions

$$B = 400 \text{ G},$$

$$\varphi_f = 1560 \text{ V},$$

$$J_c = 1 \text{ A/cm}^2, \text{ and}$$

$$\varphi_f/B^2 = 9.76 \times 10^5 \text{ V/G}^2.$$

In the interaction region the solid path corresponds to the location of the maximum beam-current interception as determined from the analyzer investigations. The circled points represent the boundaries of the beam between which at least 90% of the electrons are moving. The experimental operating conditions were

$$B = 381 \text{ G},$$

$$\varphi_f = 1445 \text{ V},$$

$$J_c = 0.65 \text{ A/cm}^2, \text{ and}$$

$$\varphi_f/B^2 = 9.97 \times 10^5 \text{ V/G}^2.$$

Since φ_f/B^2 is nearly the same in the two cases, the location of the beam at the gun-exit plane should be the same. Inspection of Fig. 10 indicates that the locations at this plane are in good agreement.

Aperture Measurements

The above investigations have been concerned only with the gross or macroscopic variations of the beam, i.e., beam-profile measurements including variation of the beam location and average space-charge density. Additional information concerning the beam can be obtained by placing an aperture system (consisting of two parallel plates) directly behind the grid wires. A small portion of the beam passes through the 0.004-in.-diam opening in the aperture plate and arrives at the deflection plate. The average local space-charge density $\langle \rho \rangle$ can be determined if the average z component of current density $\langle J_z \rangle$ and velocity $\langle \dot{z} \rangle$ of the electrons entering the aperture are known,

$$\langle \rho \rangle = \langle J_z \rangle / \langle \dot{z} \rangle. \tag{2}$$

$\langle J_z \rangle$ can be evaluated from the relation

$$\langle J_z \rangle = I_0/A, \tag{3}$$

where I_0 is the total current passing through the aperture and A is the aperture area. Evaluation of $\langle \rho \rangle$ in this manner is carried out with the aperture system located near the gun-exit plane (approximately 0.050 in. away). The current I_0 passing through the aperture is monitored for various operating conditions. In order to match the electric field at the gun exit with that in the anode–sole region, φ_f, φ_a, and φ_s are selected so that no curvature of the equipotential lines occurred in moving from the gun to the anode–sole region. The magnetic field is then increased until the deflection plate current becomes a maximum. For this condition it is assumed that the average motion of the electrons pass-
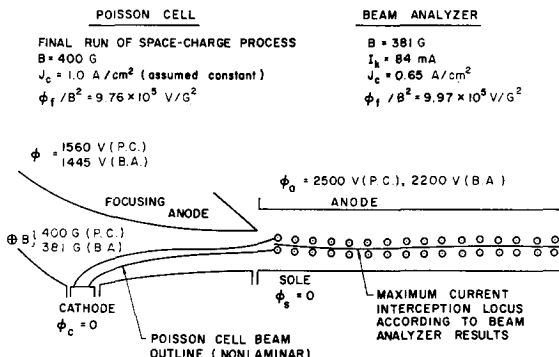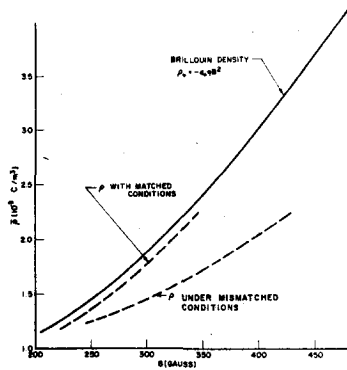
FIG. 11. Space-charge density as a function of magnetic field.

ing through the aperture is in the z direction and the average velocity is given by

$$\langle \dot{z} \rangle = (2\eta)^{\frac{1}{2}} \varphi_0, \tag{4}$$

where φ_0 is the space-charge-free voltage corresponding to the aperture location.

The results are illustrated in Fig. 11 for both matched and mismatched conditions at the gun-exit plane. The average space-charge density calculated from Eq. (2) is nearly equal to the Brillouin density for each magnetic field value with matched conditions. However, when the electric fields are mismatched, the apparent $\langle \rho \rangle$ values are much less, indicating that the electrons do not have $\langle \dot{y} \rangle = 0$ in this case. Thus the $\langle \dot{z} \rangle$ values are actually less than indicated by Eq. (4), so that the actual $\langle \rho \rangle$ is greater than shown in Fig. 11. These results demonstrate that the fields must be matched at the gun exit in order to produce a well-defined electron beam.

Attempts were made to measure the velocity distribution in the beam by observing the deflection plate current as the voltage between aperture plate and deflection plate is varied. In theory, the distribution of electron velocities should be obtainable by the proper interpretation of the current variation with voltage. However, secondary emission from the deflection plate obscured the data and precluded the possibility of obtaining the desired information.

CONCLUSIONS

An experimental beam analyzer system has been developed which allows for an analysis of crossed-field space-charge flows. The experimental data provide information concerning the gross behavior of the electron beam as it proceeds through a planar anode–sole region. The results clearly indicate the undulatory motion of the beam in the anode–sole region. The experimental cycloidal wavelengths are found to agree with the theoretical values for electrons moving in static crossed electric and magnetic fields. In general, the beams are found to be wider than the Brillouin beam for the corresponding conditions.

An evaluation of the beam distortion created by the presence of the grid wires indicated that the effect is small. This was illustrated by removal of the bias voltage to grid wire 4 and comparison of the current intercepted by wire 3 in this case with that when wire 4 has a voltage applied to it. The variation of I_3 in each case was nearly the same, with only the magnitude of I_3 being different.

There is some secondary emission which occurs when the beam strikes the grid wires, but the effect is not critical. It shows up by causing the lower potential wires which intercept the beam to have a reduced net current. In addition, secondaries emitted by the beam-intercepting wires are able to reach wires located outside of the actual beam configuration, thus indicating a wider beam than actually exists.

Comparison of the beam analyzer results with those obtained from a theoretical Poisson cell analysis indicate relatively good agreement with respect to the location of the beam at the exit plane of the gun.

The space-charge densities which were obtained from the experiments by using an aperture system indicated values in the range of 0.5 to 1.5 times the Brillouin value. However, attempts to measure the distribution of electron velocities in the beam were limited due to secondary emission problems.

In general, the crossed-field beam analyzer provides a useful method for evaluating the space-charge flow obtained from a specific electron-gun configuration. In this connection it also provides a means for adjusting various parameters (such as focusing anode voltage and magnetic field) to optimize the behavior of the electron beam. Thus the system is useful both for fundamental investigations of space-charge flow and as a tool for optimizing the performance of a given electron gun.